J Solid State Electrochem (2001) 5: 205–211
DOI 10.1007/s100080000137

ORIGINAL PAPER

Stefan Sauter · Gunther Wittstock

Local deposition and characterisation of $K_2Co[Fe(CN)_6]$ and $K_2Ni[Fe(CN)_6]$ by scanning electrochemical microscopy

Received: 2 February 2000 / Accepted: 7 April 2000 / Published online: 1 March 2001

Abstract Scanning electrochemical microscopy (SECM) is used to form local deposits of different Prussian blue analogs on macroscopic surfaces of gold and glassy carbon. Dissolution of Co and Ni sacrificial ultramicroelectrodes (UMEs) generates divalent cations in the gap between the UME and the macroscopic specimen electrode. Co^{2+} or Ni^{2+} precipitate with $[Fe(CN)_6]^{4-}$ formed by reduction of $[Fe(CN)_6]^{3-}$ at the macroelectrode. By moving the UME while generating Co^{2+} or Ni^{2+}, lines can be "drawn" with a width of 130 μm. The line width can be adjusted by reagent concentration and translation speed of the UME. Different pulse programs allow the formation of ring-shaped structures. The deposited hexacyanoferrate microstructures show catalytic activity for the reduction of Fe^{3+} which was imaged in the feedback and generation-collection modes of the SECM.

Key words Scanning electrochemical microscope · Cobalt hexacyanoferrate · Nickel hexacyanoferrate · Microstructuring · Electrocatalysis

Introduction

Electrodes modified with Prussian blue analogs have received considerable interest in recent years because of their widespread applicability. The ion exchange properties have been used for the absorption of radioactive caesium from waste waters [1, 2, 3]. Sensors for different alkaline earth metals ions, alkali metals ions, heavy metal ions and NH_4^+ are based on recording a shift of the peak potential in cyclic voltammograms (CVs) [4, 5, 6] of metal hexacyanoferrate-carbon composite electrodes [4], of metal hexacyanoferrates immobilised on electrodes [5] or of membrane electrodes [6]. The peak shift correlates with the logarithm of the analyte ion concentration. Amperometric sensors have also been investigated which are based on the electrocatalytic properties of metal hexacyanoferrates for oxidation of NH_3OH^+, NO_2^-, $S_2O_3^{2-}$, N_2H_4 [7] and H_2O_2 [8], or on the electrocatalytic reduction of Fe^{3+} [9]. The electrocatalytic oxidation of H_2O_2 has also been used to construct a glucose biosensor by combining a Prussian blue analog-modified electrode with a layer of immobilised glucose oxidase [10, 11]. Intensive investigations have been devoted to the physical properties of metal hexacyanoferrates like their electrochromic behaviour [12, 13, 14], magnetisation [15, 16, 17], the lattice contraction and expansion [18, 19] and the diffusion of ions within the hexacyanoferrate structures [20, 21].

Modification of electrode surfaces with cobalt and nickel hexacyanoferrates has been achieved by electrochemical synthesis. One route is based on performing CVs in a dilute solution of Co^{2+} or Ni^{2+} that additionally contains $[Fe(CN)_6]^{3-}$ [7, 22]. Alternatively, metal hexacyanoferrates can be obtained by galvanic deposition of Me (Me = Co, Ni) from a Me^{2+}-containing solution followed by solution exchange and a positive-going potential scan in a solution of $[Fe(CN)_6]^{3-}$ and KCl. This causes the simultaneous dissolution of the deposited metal and the formation of $[Fe(CN)_6]^{4-}$, leading to a precipitation of $K_2Me[Fe(CN)_6]$ [23].

Recently, scanning electrochemical microscopy (SECM) has become a versatile tool for imaging the local electrochemical reactivity of various surfaces ranging from composite electrodes [24, 25] and (electro)-catalytically active surfaces [26] to liquid/gas interfaces [27]. The SECM has also been used for local modification of surfaces [28]. Procedures of modification are based (1) on exploiting the inhomogeneous electric field between a microelectrode and a specimen for local electropolymerisation of conducting polymers [29], etching of metals [30] and local desorption of self-assembled monolayers [31, 32] (direct mode); (2) on local

S. Sauter · G. Wittstock (✉)
University of Leipzig, Wilhelm Ostwald Institute
of Physical and Theoretical Chemistry,
Linnéstrasse 2, 04103 Leipzig, Germany
E-mail: wittstoc@rz.uni-leipzig.de
Fax: +49-341-9736399

generation of reagents for deposition processes [33], local etching of semiconductors and metals [34], and initiating of pitting corrosion [35, 36]; or (3) on local perturbation of an equilibrium [37].

In this work a sacrificial ultramicroelectrode (UME) was used to generate divalent cations. $[Fe(CN)_6]^{4-}$ ions are simultaneously generated at the specimen electrode. In contrast to earlier research [33], the metal cations are not deposited galvanically at the specimen electrode but combine with $[Fe(CN)_6]^{4-}$ to form an insoluble precipitate (Fig. 1). Because the cation formation at the UME and the $[Fe(CN)_6]^{4-}$ generation at the sample can be influenced by separate potential programs, the deposition process can be controlled by the experimental conditions. The electrocatalytic properties of the resulting microstructures were characterised by the imaging modes of the SECM.

Experimental

Chemicals

All chemicals were of analytical grade. $K_3[Fe(CN)_6]$, $CoCl_2 \times 6H_2O$, $NiCl_2 \times 6H_2O$ and KCl were purchased from Merck (Darmstadt, Germany). Gold (99.98%), cobalt (99.9%, radius $r = 25$ μm), nickel (99.98%, $r = 12.5$ μm) and platinum wires (99.98%, $r = 12.5$ μm and 25 μm) were obtained from Goodfellow (Bad Nauheim, Germany). Experiments were performed in 0.1 M KCl solution prepared from deionised water (LiquiPure, Christ, Stuttgart, Germany).

Substrates

Macroscopic gold specimens were either glass plates coated with 50 nm Cr and 2000 nm gold or a freshly polished pen-shaped gold electrode (2 mm diameter, CH Instruments, Cordova, USA). The procedure was also tested on glassy carbon electrodes (3 mm, CH Instruments).

SECM procedures

Pt UMEs were prepared according to the procedure of Kranz et al. [38]. Co and Ni UMEs were prepared by a similar process using cobalt or nickel wires. The SECM experiments were performed using a self-built SECM [39] with a three-axis inchworm (Burleigh, Fishers, NY, USA) positioning system and a home-built bipotentiostat. The voltammetric experiments were either done at the SECM or at an Autolab PGSTAT10 potentiostat (ECO-Chemie, Utrecht, The Netherlands) at an ambient temperature of 295 ± 1 K. Electrochemical cells were completed by a saturated calomel electrode (SCE, $Hg|Hg_2Cl_2|$saturated KCl from EG&G, Munich, Germany) as reference electrode and a platinum wire (in SECM experiments) or an 1 cm^2 platinum plate (conventional cells) as the auxiliary electrode. All potentials in this paper are given with respect to the SCE.

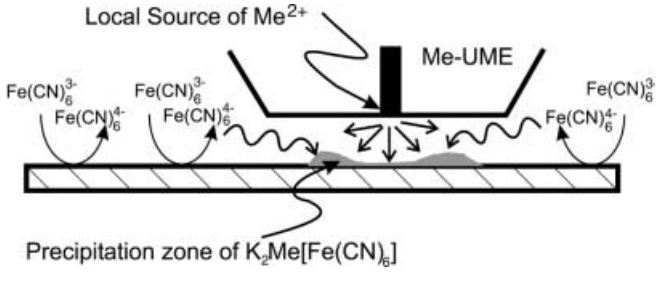

Fig. 1 Schematic of local precipitation of $K_2Me[Fe(CN)_6]$. Dissolution of a sacrificial UME generates divalent metal ions that precipitate with $[Fe(CN)_6]^{4-}$ simultaneously formed at the specimen electrode

Optical microscopy and scanning electron microscopy

Optical images of the microstructures were obtained with a Stemi 2000 microscope (Zeiss, Oberkochen, Germany) connected to a CCD camera. Scanning electron microscopic (SEM) images were recorded on DSM940 (Zeiss, Oberkochen, Germany) with 10 kV electron energy and a working distance of 5 mm.

Results and discussion

Two local precipitation procedures were developed using one or two electrochemical processes at the UME. For the technique of microdepositioning $K_2Co[Fe(CN)_6]$ or $K_2Ni[Fe(CN)_6]$ in one electrochemical step, UMEs with radii of $r_{Co} = 25$ μm or $r_{Ni} = 12.5$ μm were manufactured. One of these UME was brought to mechanical contact with the substrate and then retracted one radius of the UME. The potential was set at the tip to $E_T = -1.0$ V and at the specimen to $E_S = +1.0$ V and a $K_3[Fe(CN)_6]$ solution was filled into the cell. The potential was switched to $E_S = 0.0$ V ($[Fe(CN)_6]^{3-}$ reduction) and $E_T = +0.75$ V (metal dissolution) while the UME was moved parallel to the substrate. By doing so, a local precipitate on the sample electrode was obtained. The deposition was stopped by re-applying the starting potential of $E_T = -1.0$ V to the UME.

Precipitation occurs at the mixing zone of $[Fe(CN)_6]^{4-}$ formed at the specimen and Co^{2+} formed at the tip. Since the glass surrounding the sacrificial UME shields the diffusion of $[Fe(CN)_6]^{3-}$ to areas directly below the UME, the reduction current density at the sample is much larger outside the gap formed by the sample and the UME and its shielding. $[Fe(CN)_6]^{4-}$ diffuses into the gap where it mixes with divalent metal ions formed at the tip. Therefore, precipitation occurs mainly at the outer edge of the insulating shielding of the UME. The size of the individual lines can be influenced by the translation speed of the UME and the concentration of the $[Fe(CN)_6]^{3-}$ ions in the solution (Table 1). For the $K_2Co[Fe(CN)_6]$ precipitation, a slow UME translation and a low $[Fe(CN)_6]^{3-}$ concentration results in a very broad line because the flux of cations generated at the UME is larger than the generation rate of $[Fe(CN)_6]^{4-}$ in the immediate vicinity of the insulating shielding of the UME. Metal cations can diffuse out of the UME-sample gap and form precipitates far away from the local Me^{2+} source. By increasing the writing speed to 110 μm s^{-1}, the width is reduced by 50%. In this case the moving UME enters a solution volume that already contains enough $[Fe(CN)_6]^{4-}$ to

Table 1 Influence of translation speed and $[Fe(CN)_6]^{3-}$ concentration on the line width of the precipitate using the one-step procedure

UME from	r_T (μm)	$c([Fe(CN)_6]^{3-})$ (M)	v_T (μm s^{-1})[a]	Width of deposition
Co	25	2×10^{-3}	8	890
Co	25	2×10^{-3}	110	470
Co	25	2×10^{-3}	470	–[b]
Co	25	1×10^{-2}	110	130
Co	25	5×10^{-2}	110	–[b]
Ni	12.5	2×10^{-3}	8	850
Ni	12.5	2×10^{-3}	110	270
Ni	12.5	1×10^{-2}	110	265[c]

[a] v_T = horizontal translation speed
[b] No precipitate visible
[c] Precipitate barely visible

form precipitates with the cations generated at the UME. Further reduction of the line width is achieved by increasing the $[Fe(CN)_6]^{3-}$ concentration to 0.01 M. Figure 2 shows an optical image of an "L"-shaped deposit of $K_2Co[Fe(CN)_6]$. It was formed by moving the Co UME with a translation speed of 110 μm s^{-1} parallel to the gold substrate in a 0.01 M $K_3[Fe(CN)_6]$ + 0.1 M KCl solution. The width of the deposit is reduced to 130 μm. Further increase of the translation speed could not narrow the line width further. At such high translation speed the moving UME causes considerable convection in the surrounding solution, which leads to irregular structures or complete absence of precipitates. Likewise, a higher concentration of $[Fe(CN)_6]^{3-}$ prevented the deposition process.

When writing with the Ni UME (r_{Ni} = 12.5 μm), a similar effect was observed (Table 1). In contrast to the deposition of $K_2Co[Fe(CN)_6]$, no reduction of the size of the deposits was achieved by increasing the $[Fe(CN)_6]^{3-}$ concentration. Only the amount of deposited material was reduced, so that the structures were barely visible by optical microscopy when using a Ni UME in a 1×10^{-2} M $K_3[Fe(CN)_6]$ solution. This may be due to a smaller amount of nickel evolving at the Ni UME with r_{Ni} = 12.5 μm compared to the Co UME with r_{Co} = 25 μm.

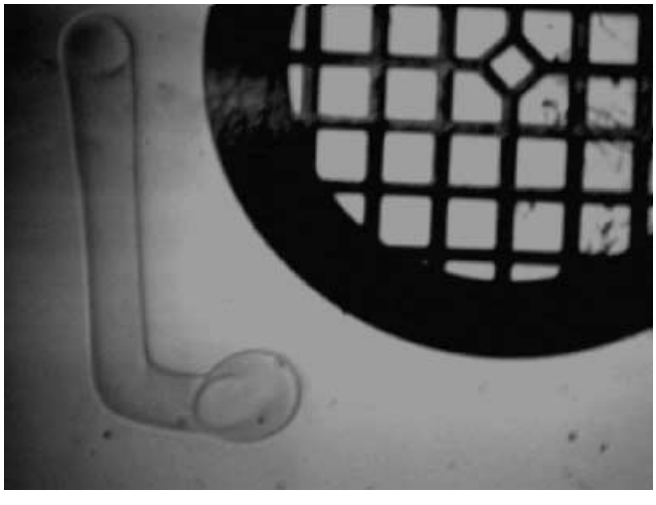

Fig. 2 Optical microscopic image of a $K_2Co[Fe(CN)_6]$ structure deposited by the one-step protocol; translation speed v_T = 110 μm s^{-1}, $c([Fe(CN)_6]^{3-})$ = 0.01 M. Also shown is a mesh with 100 lines per inch (line spacing 254 μm) as length scale

For the deposition in two electrochemical steps, first cobalt was deposited on a Pt UME (r_{Pt} = 12.5 μm) in a solution containing 1×10^{-3} M $CoCl_2$ by running a voltammetric sweep from –0.5 V to –1.15 V similar to the method described by Gao et al. [23]. The final potential was held for 1 min and the electrode withdrawn from the electrolyte while under potential control. The modified electrode was rinsed with water, transferred into a SECM cell containing air-saturated 0.1 M KCl solution and set to a potential of E_T = −1.0 V. The approach towards the substrate was monitored by measuring the negative feedback of oxygen reduction. The approach was interrupted when the UME current i_T had dropped to 50% of the diffusion controlled current in bulk solution $i_{T,\infty}$. Following this procedure, the specimen was connected as the second working electrode and set to E_S = +1.0 V. The electrolyte was changed to a 2×10^{-3} M $K_3[Fe(CN)_6]$ + 0.1 M KCl solution. The deposition of $K_2Co[Fe(CN)_6]$ was initiated by a potential step at the UME from E_T = −1.0 V to E_T = +0.75 V, dissolving the cobalt layer. After a variable time, a potential step at the specimen from E_S = +1.0 V to E_S = 0.0 V caused the reduction of $[Fe(CN)_6]^{3-}$. The UME was switched back to E_T = –1.0 V after 1 min or longer to ensure complete stripping of the deposited Co metal from the Pt UME.

The precipitates achieved with this protocol showed a different structure from those obtained with a sacrificial UME, because the amount of the divalent cation is limited by galvanic deposition of Co on the Pt UME prior to the stripping process. Because continuous writing is impossible, only spots of metal hexacyanoferrate are formed. The timing of the potential steps at the UME and at the sample determines the size and shape of the precipitates. Figure 3 shows a optical image of a $K_2Co[Fe(CN)_6]$ ring. The ring consists of $K_2Co[Fe(CN)_6]$ and was obtained by a potential step at the UME followed by a potential step at the specimen 15 s later. The outer diameter of this ring is 450 μm; its width amounts to 100 μm. The ring shape structure resembles the mixing zone of the Co^{2+} ions generated at the tip and the $[Fe(CN)_6]^{4-}$ ions formed at the sample. Because the UME shields the sample region beneath the UME and its insulating shielding, most of the $[Fe(CN)_6]^{4-}$ found in the precipitates is formed outside the UME-sample gap and diffuses into the gap. Besides the factors discussed above for the moving sacrificial UME, the time lag between metal dissolution at the UME and onset of $[Fe(CN)_6]^{4-}$ formation at the sample determines how far Co^{2+} ions can move away from the UME before precipitation can occur with $[Fe(CN)_6]^{4-}$.

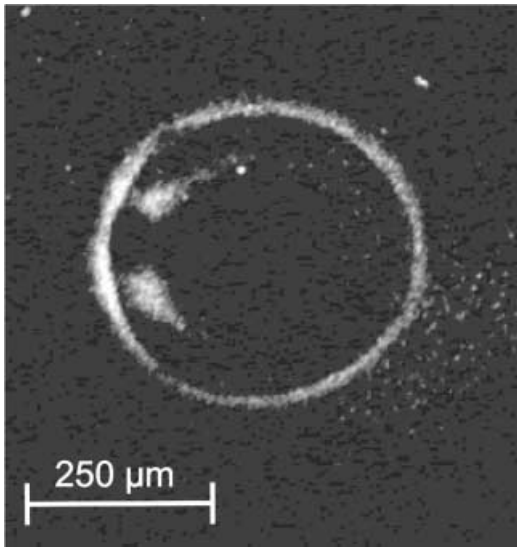

Fig. 3 Optical microscopic image of ring-shaped structure of $K_2Co[Fe(CN)_6]$ deposited by the two-step synthesis; UME switched 15 s before the sample. Ring diameter ~450 µm; ring line width ~100 µm

By changing the order of the potential steps, the diameter of the ring is reduced to about 100 µm (central feature in Fig. 4a). Although the optical image suggests that there is a ring-shaped precipitate as well, SEM images (Fig. 4b) show that there is a massive block of $K_2Co[Fe(CN)_6]$ at one side, while at the other side the ring is continued by many small discrete crystallites. This distorted radial distribution of precipitates is most likely caused by a tilt between the UME and its insulating shielding versus the specimen surface. Another SEM image (Fig. 4c) shows a change of the crystal size from the inside of the ring (bottom left) to the outside (top right). The inner region is characterised by very small and irregular crystals, followed by a zone of probably optimum growth conditions, while towards the outer perimeter only small crystallites occur. This variation in crystal morphology is probably due to different concentration ratios of Co^{2+} and $[Fe(CN)_6]^{4-}$ within the precipitation zone. There is a Co^{2+} excess during the deposition experiment in the inner part, while at the outer the $[Fe(CN)_6]^{4-}$ is in excess. In the middle part, the growth of bigger crystals indicates that the stoichiometric ratio of Co^{2+} and $[Fe(CN)_6]^{4-}$ is found there.

Layer thickness

During a scan at 100 µm s^{-1} the dissolution current at a Co UME with $r_T = 25$ µm is about 4 µA. Integration over $t = 11$ s results in a charge of $Q = 44.15$ µA s. Using Faraday's law, the molar mass of Co, $M = 58.93$ g mol^{-1}, and the density of Co, $\rho = 8.89$ g cm^{-3}, the length h of the Co wire can be calculated that dissolves within 1 s $[h = QM/(zF\rho\pi r_T^2 t)]$. This value is 70 nm s^{-1}.

An upper value of the layer thickness of the precipitated $K_2Co[Fe(CN)_6]$ can be estimated using the dissolution rate of Co (70 nm s^{-1}, corresponding to 2×10^{-11} mol s^{-1} with $r_T = 25$ µm) and estimates for the area of the precipitate in Fig. 2 (2000 µm × 130 µm = 2.6×10^{-7} m^2) and the density of $K_2Co[Fe(CN)_6]$ (4 formula units per unit cell with cell constant $a = 10.2 \times 10^{-10}$ m [40] gives 2.18 g cm^{-3}). The maximum of the deposited volume of $K_2Co[Fe(CN)_6]$ during 18 s is 5.76×10^{-8} cm^3. Thus the maximum possible layer thickness of the $K_2Co[Fe(CN)_6]$ precipitate under our experimental conditions is 220 nm. Profiles of AFM images of the border between the precipitate of Fig. 2 and the blank sample electrodes show a height of 100 nm without resolving clear steps or other regular features. SEM images of precipitates could clearly locate the film by a lower intensity of secondary electrons but did not show any regular features or crystallites like those shown in Fig. 4c. Energy dispersive X-ray emission analysis of the film and of the adjacent blank sample electrode clearly showed the presence of Fe and Co only on the modified electrode areas. We conclude that about 50% of the Co dissolved at the Co UME is actually found in the localised precipitate and that the precipitate in Fig. 2 consists of very small crystallites or even amorphous material.

Visualisation of the catalytic activity of $K_2Co[Fe(CN)_6]$

Wipf and Bard [26] have already shown the influence of heterogeneous electron-transfer rate at the substrate on SECM signals. They used the reduction of $Fe^{3+}_{(aq)}$ at gold as an example for a fast reaction, while the same reaction is slow at a glassy carbon electrode (GCE). These differences can be used to image different regions of modified electrodes. Kulesza et al. [9] showed electrocatalysis of $Fe^{3+}_{(aq)}$ reduction at a glassy carbon macroelectrode modified with hexacyanoferrates. This effect is shown in the cyclic voltammograms recorded with glassy carbon macroelectrodes (Fig. 5). The scan of the bare GCE shows the reduction of $Fe^{3+}_{(aq)}$ at 0.0 V (Fig. 5, curve 3), while at the GCE modified with $K_xCo[Fe(CN)_6]$ ($x = 1$ for oxidised and $x = 2$ for reduced states) the reduction of the $Fe^{3+}_{(aq)}$ occurs already around +0.2 V (Fig. 5, curve 1). It can be concluded that at +0.25 V the reduction of $Fe^{3+}_{(aq)}$ will be dominated by the reaction at $K_2Co[Fe(CN)_6]$. These effects are used here to visualise the electrocatalytic activity of $K_2Co[Fe(CN)_6]$ deposits on glassy carbon at constant potential $E_S = +0.25$ V. When using $Fe^{2+}_{(aq)}/Fe^{3+}_{(aq)}$ as mediator, both the generation-collection mode (GC) as well as the feedback mode (FB) [41] can be used for the SECM experiments. The oxidation/reduction of the $KCo[Fe(CN)_6]/K_2Co[Fe(CN)_6]$ film itself give rises to two pairs of signals between +0.4 V and +0.7 V. Owing to the loss of deposited material during the first cycles after preparation, the signal for the reduction of the $K_2Co[Fe(CN)_6]$ film in Fig. 5 (curve 1) is smaller than

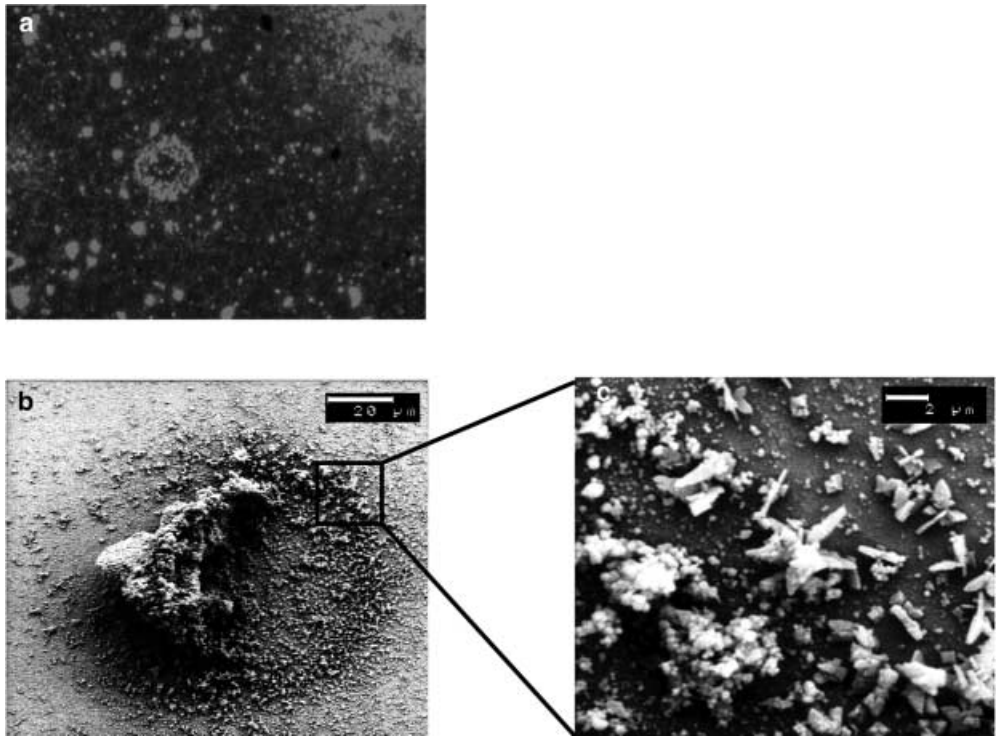

Fig. 4a–c Ring-shaped precipitate of $K_2Co[Fe(CN)_6]$ obtained by the two-step procedure. The UME switched 15 s after the substrate; ring diameter ~90 µm. **a** Optical microscopic image (precipitate is ring in the center, smaller spots around the circle are reflections from dirt particles); **b** and **c** SEM images of details

just after preparation (Fig. 5, curve 2). The signal at +0.66 V can clearly be seen in curves 1 and 2, while the second reduction signal clearly seen in curve 2 at +0.47 V merges with the rising part of the large, broad peak for the reduction of dissolved $Fe^{3+}_{(aq)}$ in Fig. 5, curve 1. The oxidation signal at +0.53 V in curve 2 corresponds to the shoulder in curve 1 at the same potential while the oxidation of $Fe^{2+}_{(aq)}$ in curve 1 results in the peak at +0.62 V.

After the deposition in one electrochemical step the deposition electrolyte was exchanged against 2 mM $FeCl_3$ + 1 M HCl + 1 M KCl solution for GC imaging. The substrate was set to a potential of $E_S = +0.25$ V and the Pt UME to $E_T = +0.8$ V in order to collect the generated $Fe^{2+}_{(aq)}$ ions. The resulting GC image (Fig. 6) reflects the catalytic activity of the deposited $K_2Co[Fe(CN)_6]$. Only at the modified regions are considerable amounts of $Fe^{2+}_{(aq)}$ generated, while low currents are found above unmodified glassy carbon. Because the $Fe^{2+}_{(aq)}$ diffuses away from the point of origin, the SECM image appears broader than the line width of the $K_2Co[Fe(CN)_6]$ precipitate as seen by optical microscopy (130 µm).

Higher lateral resolution can be expected from SECM FB images, which were carried out with a divalent iron species as mediator [2 mM $(NH_4)_2Fe(SO_4)_2$ + 0.5 M H_2SO_4 + 0.5 M K_2SO_4]. As in the GC experiments, the UME potential $E_T = +0.8$ V

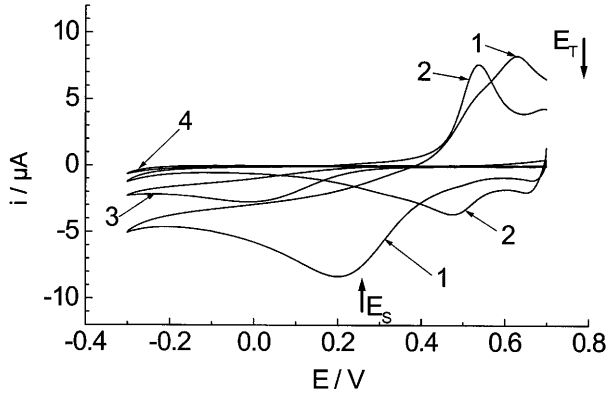

Fig. 5 Cyclic voltammograms of *1* GCE modified with $K_xCo[Fe(CN)_6]$ ($x = 1$ for oxidised and $x = 2$ for reduced states) in a solution of 2 mM $FeCl_3$ + 1 M HCl/KCl, *2* GCE modified with $K_xCo[Fe(CN)_6]$ in a solution of 1 M HCl/KCl, of *3* plain GCE in a solution of 2 mM $FeCl_3$ + 1 M HCl/KCl, and *4* plain GCE in a solution of 1 M HCl/KCl; scan rate = 0.01 V s^{-1}, $E_{start} = +0.7$ V, $E_{vertex} = -0.3$ V, $E_{final} = +0.7$ V. Modification with $K_xCo[Fe(CN)_6]$ was carried out according to [23]

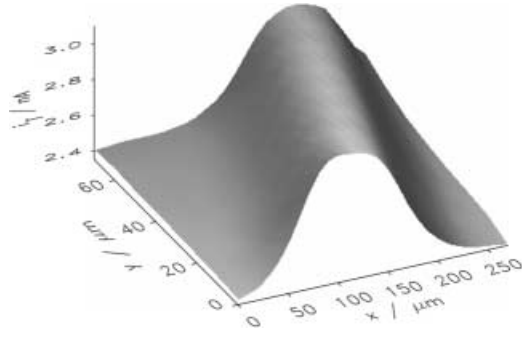

Fig. 6 SECM GC image of the electrocatalytic activity of a $K_2Co[Fe(CN)_6]$ precipitate; $r_T = 12.5$ µm; $d = 30$ µm; solution 2 mM $FeCl_3$ + 1 M HCl + 1 M KCl; $E_T = +0.8$ V; $E_S = +0.25$ V

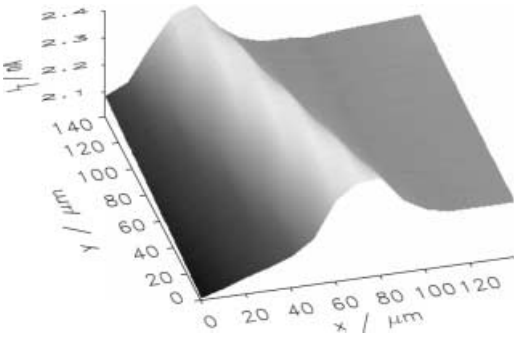

Fig. 7 SECM FB image of the electrocatalytic activity of a $K_2Co[Fe(CN)_6]$ precipitate; $r_T = 12.5$ µm; $d = 10$ µm; mediator solution 2 mM $(NH_4)_2Fe(SO_4)_2 + 0.5$ M $H_2SO_4 + 0.5$ M K_2SO_4; $E_T = +0.8$ V; $E_S = +0.25$ V

causes the oxidation of $Fe^{2+}_{(aq)}$. The re-reduction of UME-generated $Fe^{3+}_{(aq)}$ occurs at the $K_2Co[Fe(CN)_6]$-modified regions of the sample at a potential $E_S = +0.25$ V (Fig. 7). The reduction of the mediator is fast enough only at $K_2Co[Fe(CN)_6]$ so that a positive feedback due to mediator regeneration at the sample is found only when the UME is located above the deposited $K_2Co[Fe(CN)_6]$ but not when located above the bare glassy carbon. The lateral resolution of the images is improved compared to Fig. 6 because the reactant for the reaction at the sample is provided locally by the UME. The higher feedback currents can in principle also originate from a decrease of the UME-sample distance d above the protruding precipitate. Based on the GC imaging at large d (where feedback effects are negligible) and the small thickness of the precipitate (100 nm from AFM) compared to d, this can be excluded as the exclusive reason for the increased feedback currents.

Conclusion

A method was presented to precipitate Prussian blue analogs by means of SECM using two different protocols. The principle was exemplified with $K_2Ni[Fe(CN)_6]$ and $K_2Co[Fe(CN)_6]$, but it should be possible to extend it to other hexacyanometallates, for which macroscopic electrochemical surface modification procedures have been published that rely on precipitation. For continuous writing, a sacrificial UME is prepared from a metal wire with a diameter not larger than 50 µm. The metal must be electrochemically dissolvable. The dissolution rate of 70 nm s^{-1} is small compared to the radius of the Co UME. Therefore, one Co UME could be used for more than 150 s continuous writing (15,000 µm) until the surrounding glass shield was polished back to be in plane with the Co UME.

The line width of the deposits is still quite broad but should be reducible by using scavenger compounds in the bulk solution, similar to the idea introduced for several local electrochemical modification protocols [42, 43, 44, 45]. To reduce the line width of the precipitated metal hexacyanoferrrates, the effect of the insulating shielding of the sacrificial UMEs and the benefit of pulsed dissolution of the metal from the UME is currently being explored.

The catalytic activity of these precipitates can be investigated using the SECM as an imaging tool with $Fe^{2+}_{(aq)}$ as the species reduced at the catalytically active $K_2Co[Fe(CN)_6]$. FB images showed a better lateral resolution than corresponding GC images. The combination of microprecipitation and imaging holds great promise for creating miniaturised functional structures.

Acknowledgements The authors thank Dr. G. Wagner (Institute for Mineralogy, Crystallography and Material Science, University of Leipzig) for the SEM measurements. S. Sauter acknowledges the Deutsche Forschungsgemeinschaft for financial support within the Graduate Course GRK152/3 "Physical Chemistry of the Surfaces and Interfaces".

References

1. Mimura H, Kimura M, Akiba K, Onodera Y (1999) Sep Sci Technol 34:17
2. Clarke TD, Wai CM (1998) Anal Chem 70:3708
3. Ayrault S, Jimenez B, Garnier E, Fedoroff M, Jones DJ, Loos-Neskovic C (1998) J Solid State Chem 141:475
4. Düssel H, Dostal A, Scholz F (1996) Fresenius J Anal Chem 355:21
5. Hermes M, Scholz F (1997) J Solid State Electrochem 1:215
6. Tani Y, Eun H, Umezawa Y (1998) Electrochim Acta 43:3431
7. Chen SM (1998) Electrochim Acta 43:3359
8. Lin MS, Tseng TF, Shih WC (1998) Analyst 123:159
9. Kulesza PJ, Brajter K, Dabek-Zlotorzynska E (1987) Anal Chem 59:2776
10. Karyakin AA, Gitelmacher OV, Karyakina EE (1995) Anal Chem 67:2419
11. Lin MS, Shih WC (1999) Anal Chim Acta 381:183
12. Monk PMS, Mortimer RJ, Rosseinsky DR (1995) Electrochromism. VCH, Weinheim, chap 6
13. Kulesza PJ, Malik MA, Miecznikowski K, Wolkiewicz A, Zamponi S, Berrettoni M, Marassi R (1996) J Electrochem Soc 143:L10
14. Cataldi TRI, De Benedetto GE, Campa C (1998) J Electroanal Chem 437:93
15. Sato O, Iyoda T, Fujishima A, Hashimoto K (1996) Science 272:704
16. Sato O, Einaga Y, Iyoda T, Fujishima A, Hashimoto K (1997) J Phys Chem B 101:3903
17. Yoshizawa K, Mohri F, Nuspl G, Yamabe T (1998) J Phys Chem B 102:5432
18. Dostal A, Meyer B, Scholz F, Schröder U, Bond AM, Marken F, Shaw SJ (1995) J Phys Chem 99:2096
19. Dostal A, Kauschka G, Reddy SJ, Scholz F (1996) J Electroanal Chem 406:155
20. Kahlert H, Retter U, Lohse H, Siegler K, Scholz F (1998) J Phys Chem B 102:8757
21. Malik MA, Horanyi G, Kulesza PJ, Inzelt G, Kertesz V, Schmidt R, Czirok E (1998) J Electroanal Chem 452:57
22. Jiang M, Zhou X, Zhao Z (1991) Ber Bunsenges Phys Chem 95:720
23. Gao Z, Wang G, Li P, Zhao Z (1991) Electrochim Acta 36:147
24. Wipf DO, Bard AJ, Tallman DE (1993) Anal Chem 65:1373
25. Wittstock G, Gründig B, Strehlitz B, Zimmer K (1998) Electroanalysis 10:526
26. Wipf DO, Bard AJ (1991) J Electrochem Soc 138:469
27. Slevin CJ, Ryley S, Walten DJ, Unwin PR (1998) Langmuir 19:5331

28. Mandler D, Meltzer S, Shohat I (1996) Isr J Chem 36:73
29. Kranz C, Gaub HE, Schuhmann W (1996) Adv Mater 8:634
30. Hüsser OE, Craston DH, Bard AJ (1989) J Electrochem Soc 135:785
31. Wittstock G, Hesse R, Schuhmann W (1997) Electroanalysis 9:746
32. Wilhelm T, Wittstock G (2000) Microchim Acta 133:1–9
33. Meltzer S, Mandler D (1995) J Electrochem Soc 6:82
34. Shiku H, Uchida I, Matsue T (1997) Langmuir 13:7239
35. Wipf DO (1994) Colloids Surf A 93:251
36. Still JW, Wipf DO (1997) J Electrochem Soc 144:2657
37. Shohat I, Mandler D (1994) J Electrochem Soc 141:995
38. Kranz C, Ludwig M, Gaub HE, Schuhmann W (1995) Adv Mater 7:568
39. Wittstock G, Emons H, Ridgway TH, Blubaugh EA, Heineman WR (1994) Anal Chim Acta 298:285
40. Sharpe AG (1976) The chemistry of cyano complexes of the transition metals. Academic Press, London, p 121
41. Bard AJ, Fan FRF, Kwak J, Lev O (1989) Anal Chem 61:132
42. Tian Z, Fen Z, Tian Z, Zhou X, Mu J, Li C, Lin H, Ren B; Xie Z, Hu W (1992) Faraday Discuss Chem Soc 94:37
43. Borgwarth K, Ricken C, Ebling DG Heinze J (1995) Ber Bunsenges Phys Chem 99:1421
44. Zu Y, Xie L, Mao B, Tian Z (1998) Electrochim Acta 43: 1683
45. Borgwarth K, Heinze J (1999) J Electrochem Soc 146:3285